Journal of Alloys and Compounds 686 (2016) 733–743

Contents lists available at ScienceDirect

Journal of Alloys and Compounds

journal homepage: http://www.elsevier.com/locate/jalcom

Multichannel hollow structure for improved electrochemical performance of TiO_2/Carbon composite nanofibers as anodes for lithium ion batteries

Luis Zuniga, Victor Agubra, David Flores, Howard Campos, Jahaziel Villareal, Mataz Alcoutlabi*

Department of Mechanical Engineering, University of Texas, Rio Grande Valley, Edinburg, TX 78539, USA

ARTICLE INFO

Article history:
Received 22 April 2016
Received in revised form
8 June 2016
Accepted 9 June 2016
Available online 11 June 2016

Keywords:
Nanofibers
Forcespinning
Anodes
Lithium ion battery
TiO2
Composite

ABSTRACT

With nanofibers receiving much attention in the application of lithium ion batteries (LIBs), we herein report the use of multichannel hollow nanofibers composed of TiO_2 and Carbon as a binder-free anode for LIBs. The nanofibers were produced by the Forcespinning® of an emulsion precursor solution composed of Polyvinylpyrrolidone (PVP), Titanium (IV) butoxide, ethanol, acetic acid, and mineral oil. The as-prepared precursor nanofibers were subjected to a thermal treatment by first stabilizing in air at 280 °C followed by carbonizing at 550 °C under an argon atmosphere to form TiO_2/C composite multichannel hollow nanofibers without the need for a sacrificial polymer to produce this morphology. This fibers' hollow structure resulted in improved electrochemical performance when compared to non-hollow fibers. These hollow fibers also showed excellent cycling performance with a specific capacity of 228.9 $mAhg^{-1}$ at a current density of 100 mAg^{-1} while maintaining a Coulombic efficiency of ~98% after 100 cycles compared to the TiO_2/C non-hollow fibers which showed a capacity of 61.4 $mAhg^{-1}$. These composite hollow nanofibers show a great promise as alternative anode materials for next generation LIBs.

1. Introduction

During the past three decades, lithium-ion batteries have received much attention as an alternative clean source for energy storage in the automotive industry as well as a replacement for other battery chemistries such as NiCd and Lead Acid batteries [1–3]. Although there have been great advances in improving the energy and power density of LIBs, there is still much room for improvement to develop higher performing and safer batteries [4–7]. One of the ways to improve the performance and safety of LIBs is to use alternative materials such as nanostructured anodes [8–11] to replace the commercial graphite anode, which has low energy density and often prone to dendrite formation that normally cause battery thermal runaway [12–14]. Metals and metal oxides such as Titanium dioxide (TiO_2), Tin dioxide (SnO_2), and α-iron oxide (a-Fe2O_3) and others, have recently been investigated as potential candidates for high performance anode materials in LIBs [15–22].

Among these metal oxides, TiO_2 has shown great potential as a good anode material [23–25]. The choice of TiO_2 has been largely due to the many attributes; abundance, low-cost, environmental friendliness, and improved power and energy density [26,27]. Although there are many phases of TiO_2 such as; anatase, rutile, brookite, and TiO_2 (B) (bronze), the most desirable is the anatase phase due to the unique crystal structure and established synthetic conditions [23]. Unlike electrodes with amorphous structures, anodes with crystalline structure and good morphology are preferred for use in LIBs due to the fact that their structural integrity is preserved during prolonged charge/discharge cycles. TiO_2 based anodes exhibit good rate capability with low volume change (<4%) during repeated charge/discharge cycles due to their good structural stability (layered crystalline structure) mechanism [28]. In addition, TiO_2 anode shows higher Li insertion potential (1.5–1.8 V vs. Li/Li+) than the commercialized carbon anode materials [29]. However, some of the drawbacks for this material are its poor electron transport, low electrical conductivity [30] and poor cycling performance when compared to the commercial graphite, mostly

* Corresponding author.
E-mail address: mataz.alcoutlabi@utrgv.edu (M. Alcoutlabi).

http://dx.doi.org/10.1016/j.jallcom.2016.06.089
0925-8388/

due to its high irreversible capacity at the first cycle.

Several approaches have been designed and developed to mitigate these drawbacks of the TiO_2. One of these approaches involves microstructural manipulation; creating nanospheres, nanofibers, nanoflakes, and nanopowders of TiO_2 to improve the electrochemical performance [20,31,32]. Among these design techniques, perhaps the design and use of one-dimensional (1D) nanostructures such as TiO_2 nanofibers are the most popular methods employed to improve the electrochemical performance of TiO_2 based anodes [18,23,33–35]. Some of the attractive attributes of the nanofibers are the high surface area, higher aspect ratio, and porous microstructure. A combination of these features provides an increase in reactive sites and diffusion path for Li^+. In addition, depending on the thermal treatment of these nanofibers, flexible free-standing nanofibers could be obtained [36,37]. In this case, they are used as binder-free anodes to eliminate the need for insulating materials in the electrode (i.e. binding agents) which effectively reduces the mass of the electrode, unlike in the case of anodes made of powder nanoparticles, nanoflakes, or nanospheres where binding agents are necessary.

In this work, we seek to improve the electrochemical performance of TiO_2 by fabricating hollow TiO_2/C composite nanofiber anodes using a facile method Forcespinning® followed by subsequent thermal treatment. The effect of fiber microstructure on the electrochemical performance of these hollow fiber anodes is evaluated by comparing them to non-hollow fibers. The Forcespinning® process was chosen to produce the composite nanofibers due to its high fiber yield and ease of operation [38–41]. After Forcespinning®, the as-collected precursor nanofibers were calcined to produce TiO_2/C composite nanofibers for use as binder-free anodes in lithium-ion batteries.

2. Experimental

2.1. Materials

Poly(vinylpyrrolidone) with average Mw of 180,000, Acetic acid (≥99%), Ethanol (200 proof), and Titanium(IV) butoxide were all purchased from Sigma-Aldrich USA, while the mineral oil (Swan) was purchased from Roberts Pharmaceutical Corp. The commercial lithium foil, lithium hexafluorophosphate ($LiPF_6$), ethylene carbonate (EC), and dimethyl carbonate (DMC) were purchased from MTI Corp. USA.

2.2. Preparation of TiO_2/Carbon fibrous mats

In order to prepare the precursor solution for the TiO_2/C composite nanofibers, 15 wt% of the PVP was added to a 10:1 (by weight) ratio of Ethanol to Acetic Acid. The solution was then mechanically mixed using magnetic stirring for 4 h. Once the PVP/Ethanol/Acid formed a homogeneous solution, Titanium (IV) butoxide was added with a ratio of 17:4 (by weight) Titanium to PVP, and magnetically stirred for 2 h. Finally, 3 g of mineral oil were added dropwise while stirring to form an emulsion solution. Another precursor solution was prepared just as the first with the exception of adding mineral oil to be used as a control sample. Nanofibers were made by the Forcespinning® method of the precursor solutions. Fiber jets are formed at high spinneret rotational speeds of up to 20,000 rpm. An amount of 2 mL of the prepared solution was injected into the needle-based spinneret equipped with 30 gauge half-inch regular bevel needles. The rotational speed of the spinneret was kept at 7000 rpm. The produced fibers were deposited on a spun-bond polypropylene substrate using a vacuum collecting system. Fig. 1 shows a schematic and actual view of the Forcespinning® collecting system. The vacuum collecting system was rotated 90° after each run while changing the needles after each run. The fiber mat was removed from the substrate and dried at 120 °C in a vacuum oven for 12 h prior to carbonization. After drying, the nanofibers were then stabilized in air at 280 °C for 5 h (with a heating rate of 3°C/min), followed by carbonization at 550 °C for 5 h in an argon atmosphere to obtain a TiO_2/C composite nanofiber mat.

2.3. Electrochemical performance evaluation

The electrochemical performance of the TiO_2/C composite nanofiber anodes was performed using 2032 coin-type cells. The TiO_2/C anode thickness was approximately 40–60 μm with a weight average in the range of 3–6 mg. Lithium metal was used as the counter electrode with glass microfibers as the separator. The electrolyte used was a 1 M $LiPF_6$ salt in ethylene carbonate (EC)/dimethyl carbonate (DMC) (1:1 v/v) solvent. The cells were then assembled in an argon-filled glove box (Mbraun, USA) with O_2 and H_2O concentrations of <0.5 ppm. The electrochemical performance was evaluated by carrying out galvanostatic charge–discharge experiments at a current density of 100 mAg^{-1} between 0.05 and 3.0 V. The specific charge/discharge capacities were calculated based on the mass of the of the nanofiber anodes. The cyclic voltammetry and electrochemical impedance experiments were carried out using electrochemical impedance spectroscopy (Autolab 128 N) with a scan rate of 0.1 mVs^{-1} and at a frequency of 0.1 Hz and 1 kHz, respectively.

3. Results and discussion

3.1. Morphology

The nanofiber mat from the TiO_2/C composite was analyzed using Scanning Electron Microscopy. Figs. 2 and 3 show the nanofiber microstructure for the solutions containing mineral oil and the one without, after carbonization at 550 °C in an argon atmosphere. To further analyze the morphology and surface structure of the produced TiO_2/C composite fibers, Brunauer, Emmett and Teller (BET) analysis was carried out to analyze surface area, pore volume and pore size for both the TiO_2/C fibers with and without oil using Micromeritics ASAP 2020 (Table 1 and Fig. 4). The presence of the mineral oil in the fiber matrix acted as a sacrificial component. During the Forcespinning® process, the oil microbeads in the solution droplet stretched along with the fibers. These long strings of oil get burnt off during the carbonization process thus leaving a hollow microstructure in their place. This process created the multichannel hollow structure that is observed in the fibers containing mineral oil and absent in the fibers without the mineral oil as shown in Fig. 7. These structures were confirmed in the (BET) analysis shown in Table 1. From this table we can see the difference between the samples without oil and with oil. While the sample without oil had a surface area of 61 m^2/g, the sample with oil showed an increased surface area of 123.31 m^2/g. There was also an increase in the pore size and pore volume in the sample with oil compared to without oil. Due to this increase in surface area we can also observe from Fig. 4 how the volume adsorbed during the BET analysis was much greater in the fibers with oil than those without. Elemental and thermogravimetric analyses of the composite TiO_2/C nanofibers were performed and are shown in Fig. 5 and Fig. 6. The elemental analysis results demonstrate the fibers predominantly consist of TiO_2 and carbon. It also showed that the nanofibers consisted of carbon matrix fibers with evenly dispersed TiO_2 nanoparticles embedded within the carbon matrix as well as on the surface. The thermogravimetric analysis (TGA) was used to determine the actual weight of carbon in the TiO_2/C composite matrix.

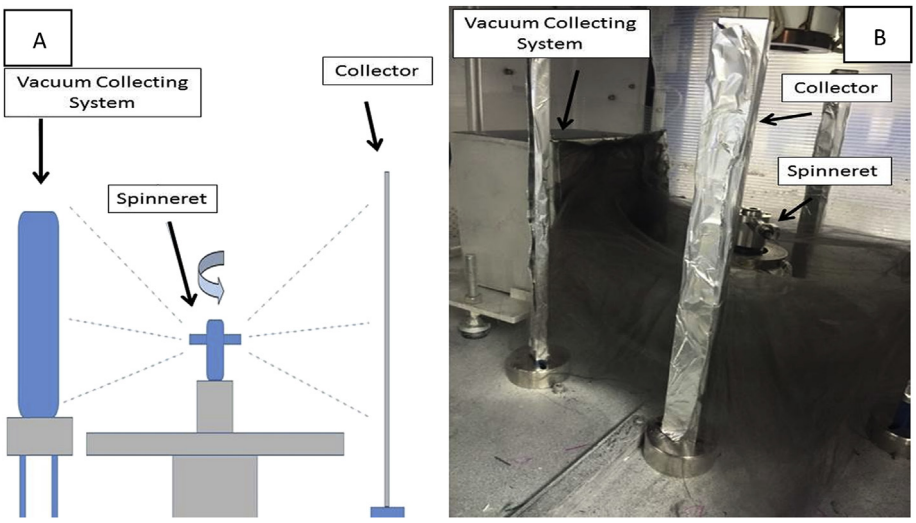

Fig. 1. Schematic representation (A) and actual view (B) of the vacuum collecting system.

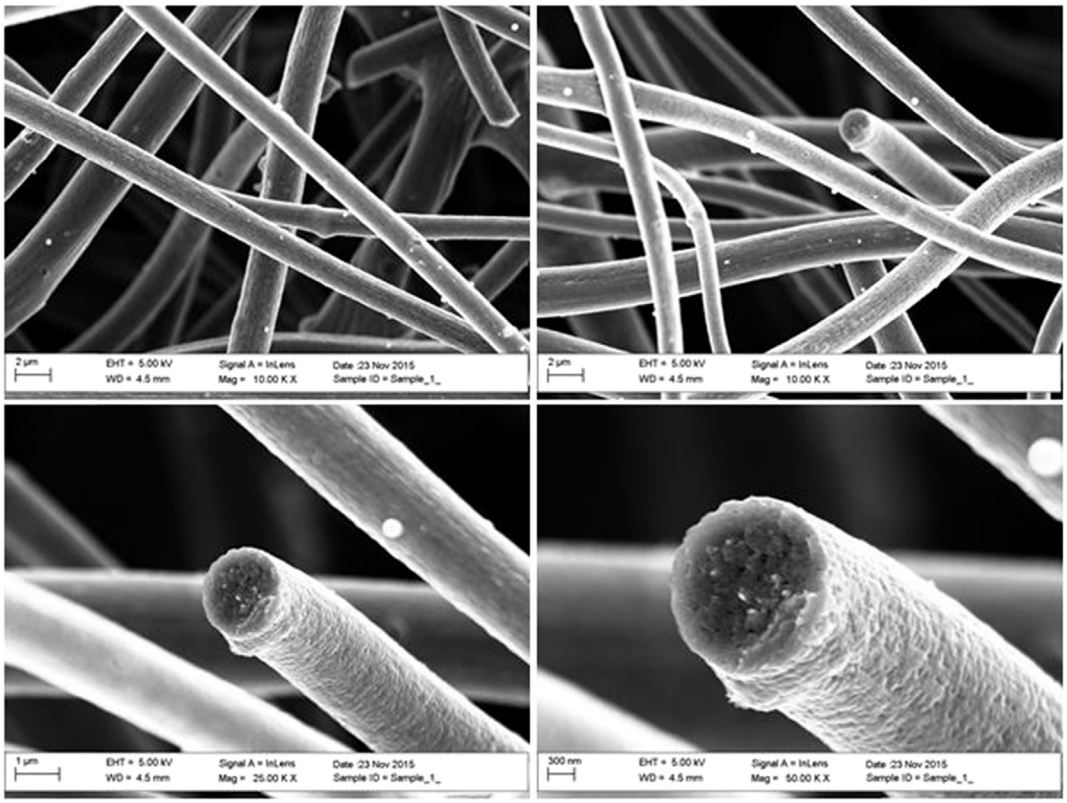

Fig. 2. SEM images of the non-hollow TiO_2/C composite nanofibers.

Based on Fig. 6, it can be seen that both the non-hollow fibers and the hollow fibers showed a multi-step decomposition process. An initial loss of ~8% and ~12% weight was observed for the non-hollow and hollow fibers respectively. This initial weight loss was attributed to the removal of physically absorbed water from the fibers. The relatively higher loss of weight for the hollow fiber was from both the removal of water and the mineral oil. At a temperature between 160 °C and 410 °C, there was a multistage decomposition that could be attributed to the polymer (PVP) which recorded a weight loss of ~34%. The oxidation of carbon was observed above 410 °C, and beyond 580 °C, thereafter the weight loss remains steady for both hollow and non-hollow fibers. The TGA results indicate that the TiO_2/C fibers contained ~69% and ~51% of carbon for the fibers without and with mineral oil, respectively.

3.2. Surface analysis: XPS

To evaluate the composition of the surface compounds on the TiO_2/C nanofibers, a high resolution XPS analysis was carried out as shown in Fig. 8. To obtain enough information on the surface

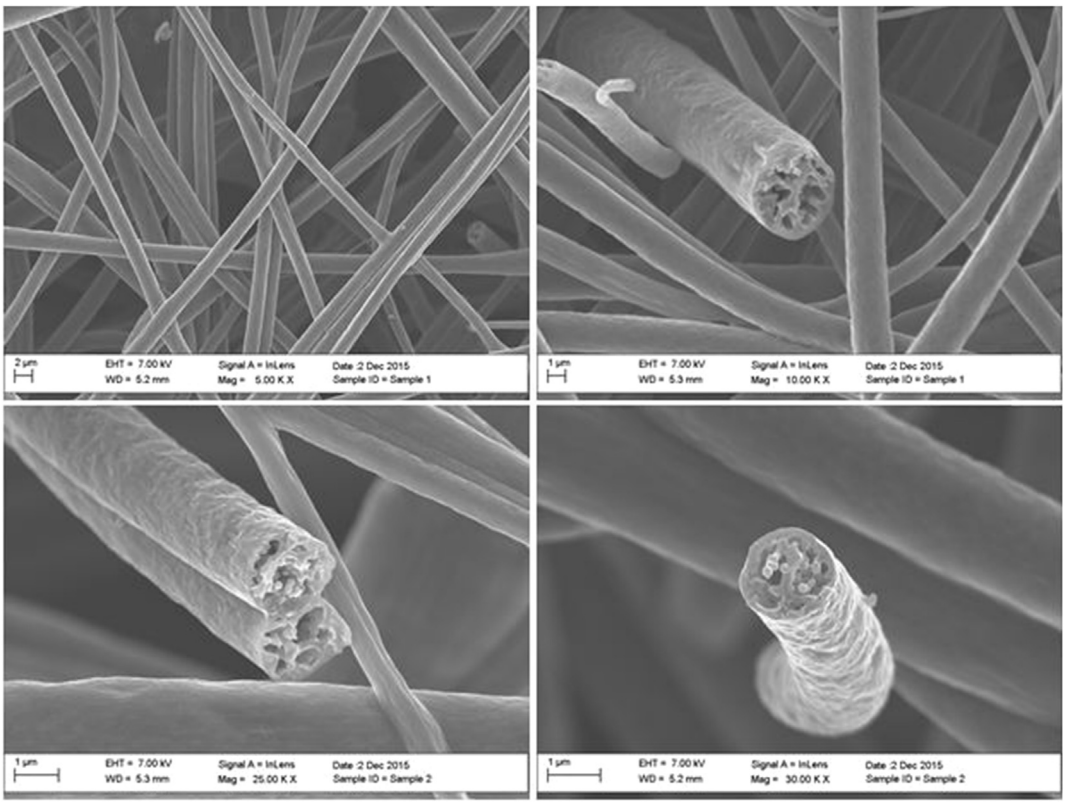

Fig. 3. SEM images of the multichannel hollow TiO_2/C composite nanofibers.

Table 1
BET analysis of TiO_2/C composite nanofibers.

Sample	TiO_2 without oil	TiO_2 with oil
Pore Size (Å)	20.9457	23.1871
Pore Volume (cm^3/g)	0.031962	0.07148
Surface Area (m^2/g)	61.037	123.3105

compounds, depth profiling instead of the regular point analysis was used. It was observed from the survey spectra that the most dominant peaks were those for titanium, oxygen, and carbon (i.e.Ti2p, O1s, and C1s) at binding energies of ~458.6, ~529.3, and ~284 eV respectively. The sharp carbon peak at binding energy of ~284 eV, reflects the predominate composition of the carbon in the fibers. The peaks shown for Ti2p correspond to Ti 2p3/2 and Ti 2p1/2, and are shown at binding energies of 458.6 eV and 463.6 eV respectively. These results for the TiO_2 peaks are in agreement with results from literature [34]. Finally the O1s showed a sharp peak at a binding energy of ~529.3 eV, and a broader peak at ~532 eV. The sharp peak corresponds to the Ti–O bond while the broader peak to that of H–O and C–O bonds [34]. The addition of mineral oil to one of the solutions had absolutely no effect on the surface analysis

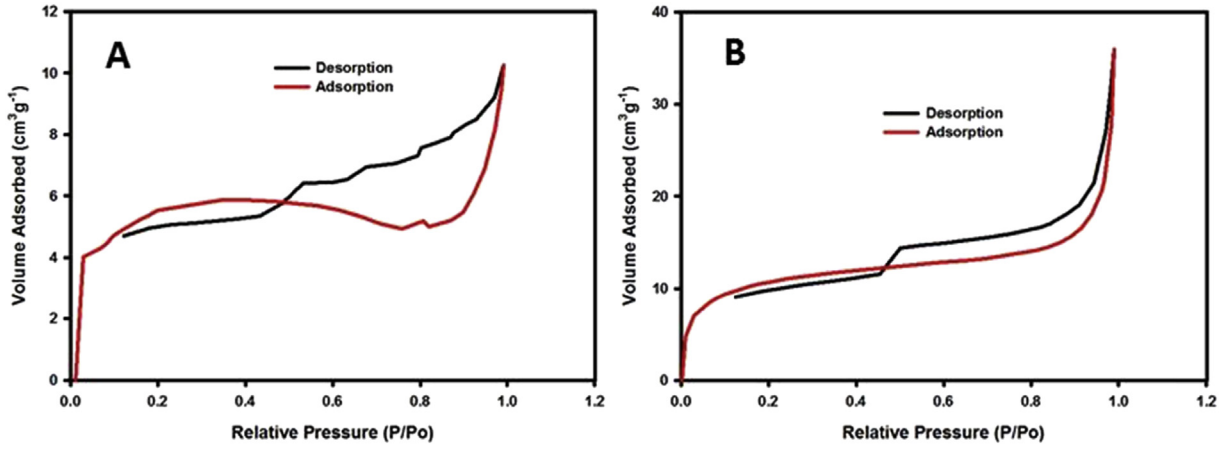

Fig. 4. Adsorption/Desorption for the non-hollow (A) and hollow (B) TiO_2/C composite nanofibers.

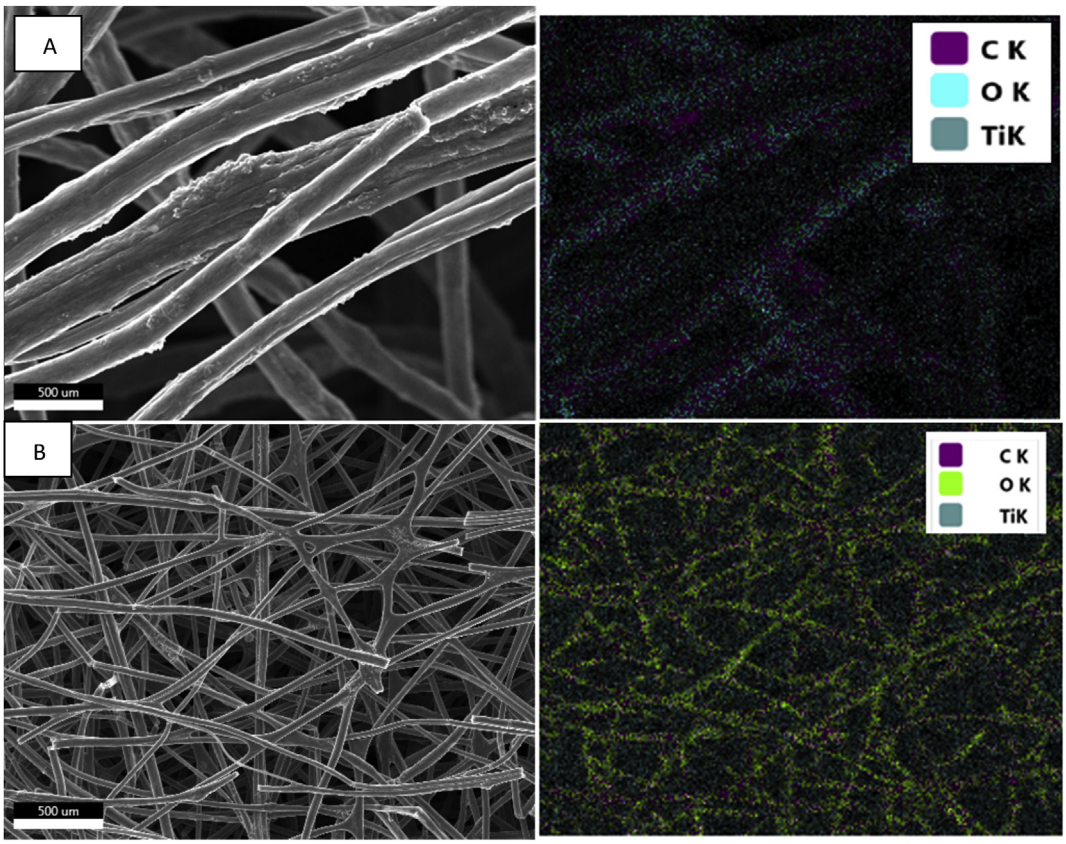

Fig. 5. Elemental analysis (EDS) for TiO_2/C composite nanofibers without mineral oil (A) and with mineral oil (B).

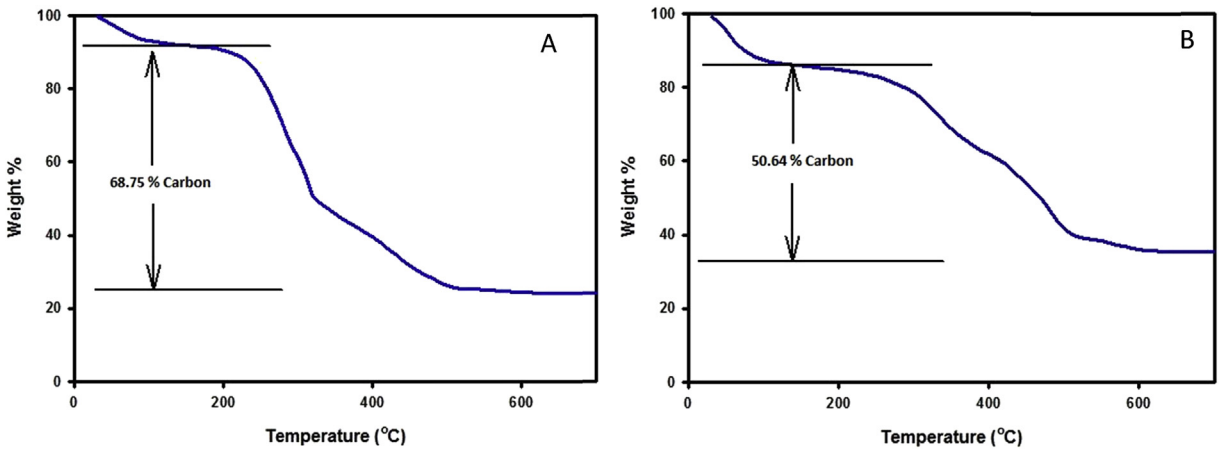

Fig. 6. Thermogravimetric analysis (TGA) for the precursor nanofibers without mineral oil (A) and with mineral oil (B).

with the results for both samples being identical, eliminating the need to provide separate figures for the two categories.

3.3. Crystal structure analysis

The crystal structure for both the multichannel and non-hollow composite fibers was analyzed using X-ray diffraction (XRD). The XRD results show a highly crystalline structure with a pure anatase phase of TiO_2 in the composite fibers (Fig. 9) based on the indexing used (JCPDS 73-1764) and comparing to pure anatase phase TiO_2 in literature [23]. The addition of mineral oil to the precursor solution had no effect on the crystal structure, as there was no noticeable difference in the crystal structure for both hollow and non-hollow fibers. This highly crystalline structure with the absence of any amorphous peaks leads to conclude that during the carbonization in argon at 550 °C the PVP polymer was fully converted into crystalline carbon, while the Titanium (IV) butoxide was oxidized to form the anatase TiO_2.

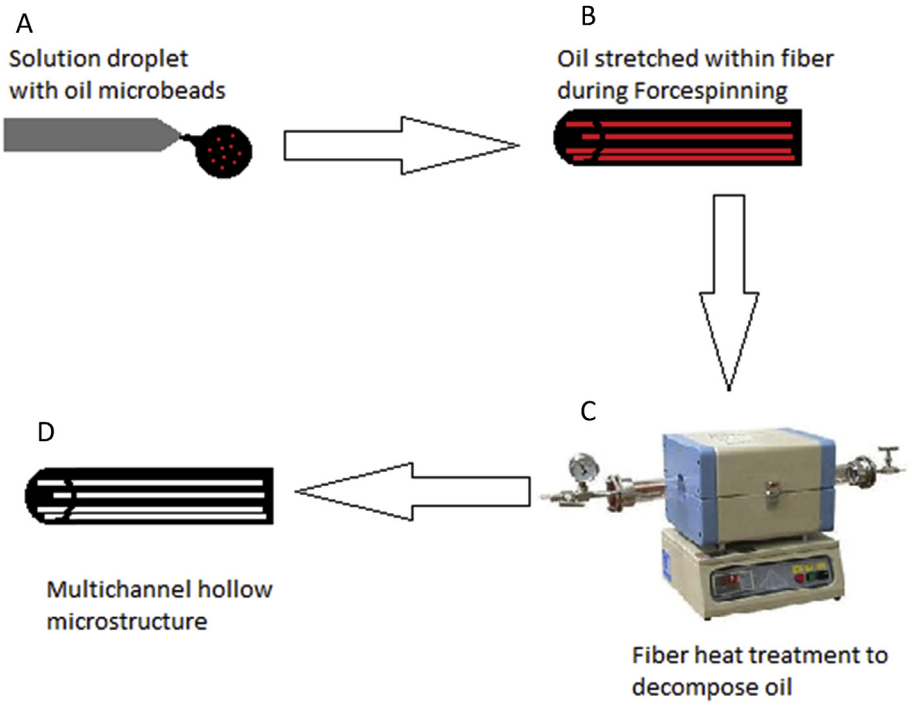

Fig. 7. Schematic of the process to create the multichannel hollow microstructure within the TiO_2/C nanofibers. (A) A solution droplet containing mineral oil microbeads as it is forced through the spinneret needle. (B) Mineral oil stretched within fibers during the Forcespinning® process. (C) Heat treatment of nanofibers carried out in a tube furnace to carbonize fibers and decompose mineral oil. (D) The multichannel hollow microstructure was obtained due to voids left from mineral oil decomposition.

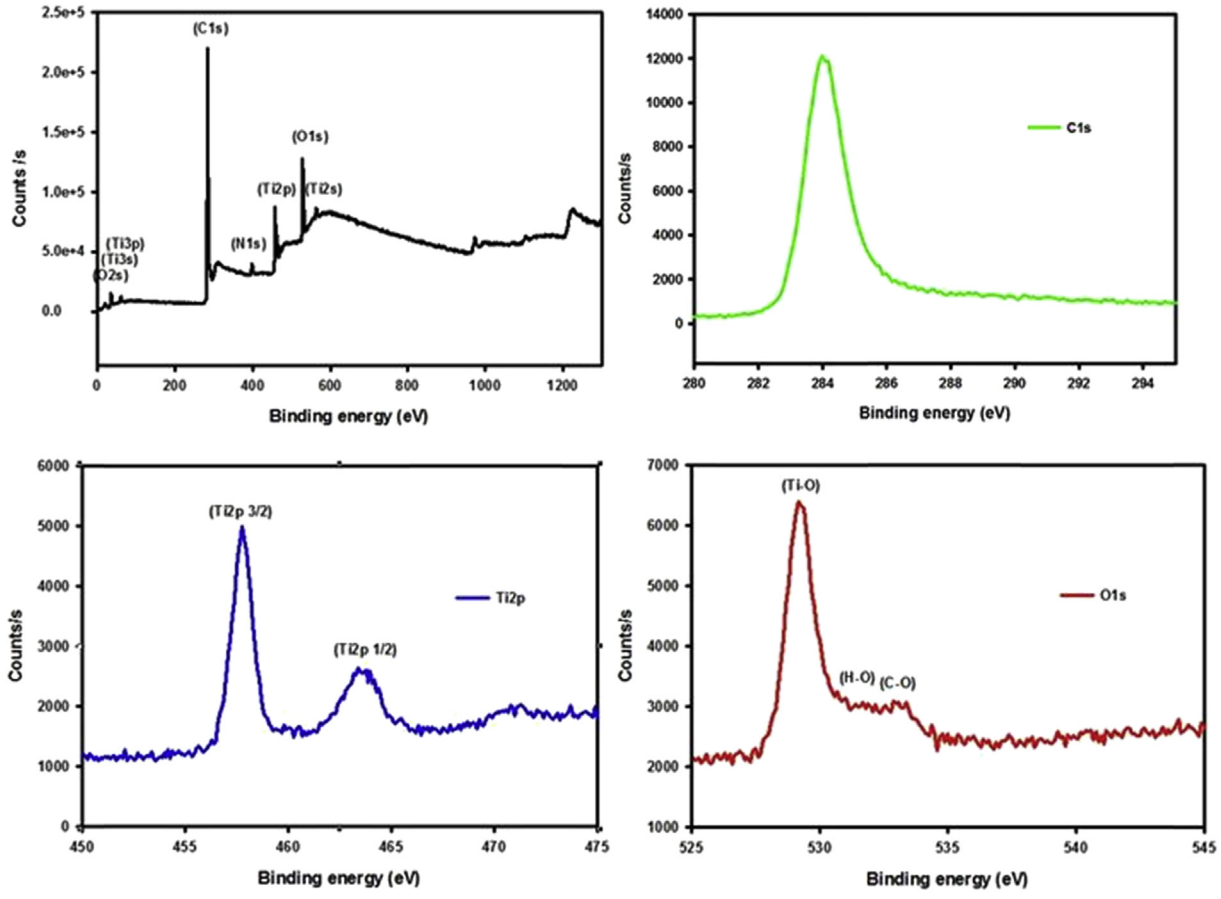

Fig. 8. XPS spectra of O1s, C1s, and Ti2p and survey spectra for the TiO_2/C composite nanofibers.

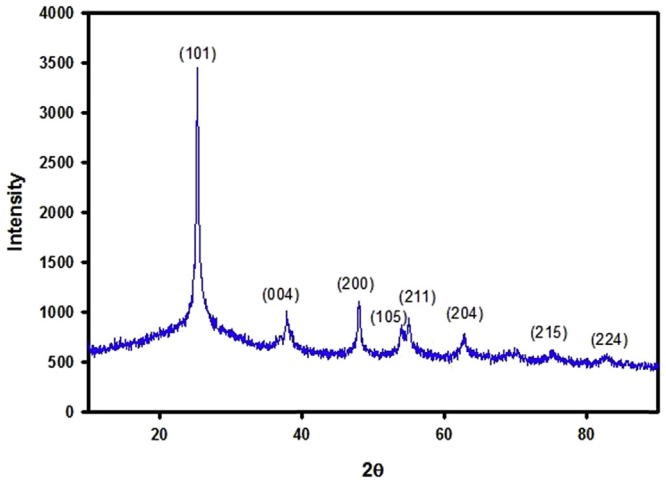

Fig. 9. XRD pattern for carbonized TiO_2/C composite nanofibers indexed using (JCPDS 73-1764). Due to the higher percentage of carbon compared to TiO_2, these characteristic peaks were not apparent [42].

4. Electrochemical analysis

4.1. Cyclic voltammetry

To understand the interaction of the Li^+ in the TiO_2/C structure, cyclic voltammograms (CV) for the cells with containing the anodes from both non-hollow and hollow fibers were evaluated for the 1st four scans, and are shown in Fig. 10. For the cell with the non-hollow fibers there was a very broad small peak during the cathodic scan (corresponding to Li^+ insertion) showing a reduction reaction at 1.0 V (i.e. denoted as R1). This broad peak is often attributed to the formation of the solid electrolyte interphase (SEI) layer as well as reduction reaction from Ti^{4+} to Ti^{3+}. The same peak was also observed in the cell with the hollow fibers (i.e. denoted as R2) but was more pronounced than that observed for the cell with the non-hollow fibers, and also had a slight shift in voltage ~0.7 V. The increase of intensity in the peak could be a result of more reaction sites for the reduction reaction between the Li^+ and TiO_2 due to the increase in surface area in the hollow fibers. During the anodic scan (Li^+ extraction) a peak was shown for both cells containing the non-hollow and hollow fibers (i.e. denoted as O1 and O2 respectively). This peak showed the oxidation reaction converting Ti^{3+} back to Ti^{4+}. The sharpness of the peak was more pronounced in the cell with hollow fibers and also has a slight shift in potential. The peak's increase in sharpness can once again be a confirmation of the increase in reactive sites due to the multichannel hollow morphology. The presence of these two peaks confirms the two phase reaction mechanism of Li^+ insertion and extraction during charge and discharge. The shift in potential in the later cycles could be attributed to the structural rearrangement of TiO_2 in the carbon matrix during the alloying/de-alloying and intercalation reactions caused by Li^+ insertion and extraction as shown in Equations (1) and (2). The lack of the characteristic TiO_2 peaks in the CV scans is due to the addition of carbon in the nanofibers. Due to the higher percentage of carbon compared to TiO_2, these characteristic peaks were not apparent [42].

$$TiO_2 + XLi^+ + Xe^- \leftrightarrow Li_xTiO_2 \quad (1)$$

$$6C + XLi^+ + Xe^- \leftrightarrow LiC_6 \quad (2)$$

4.2. Electrochemical performance

The storage/cycling performance of the TiO_2/C composite anode was investigated at room temperature (Fig. 11). The anode from the hollow TiO_2/C fibers showed an initial discharge capacity of 550 $mAhg^{-1}$ compared to 321 $mAhg^{-1}$ from the non-hollow fiber anode. The first charge capacity for both the non-hollow and hollow fiber anodes exhibited a large decrease in specific capacity. This characteristic is common among metal oxides and is attributed to the formation of the SEI layer. This phenomenon usually results in low initial coulombic efficiency [43,44]. Subsequently, the capacity of the non-hollow fiber anode showed a capacity fade of 38.2 $mAhg^{-1}$ between the 1st and 10th cycle. Thereafter, the anode capacity remained steady beyond the 10th cycle. Similarly, for the hollow fiber anode, there was a capacity fade of 70.7 $mAhg^{-1}$ between 1st and 10th cycle. However, unlike the non-hollow fibers, after the 10th cycle the capacity begins to be recovered increasing from 177.9 $mAhg^{-1}$ at the 10th to 192.3 $mAhg^{-1}$ at the 50th cycle. The capacity continues to increase showing a larger change between the 50th and 100th cycles increasing from 192.3 to 228.9 $mAhg^{-1}$. This capacity recovery could be attributed to the increase in reactive sites of the hollow fibers allowing for more Ti^+ to react as cycles increase.

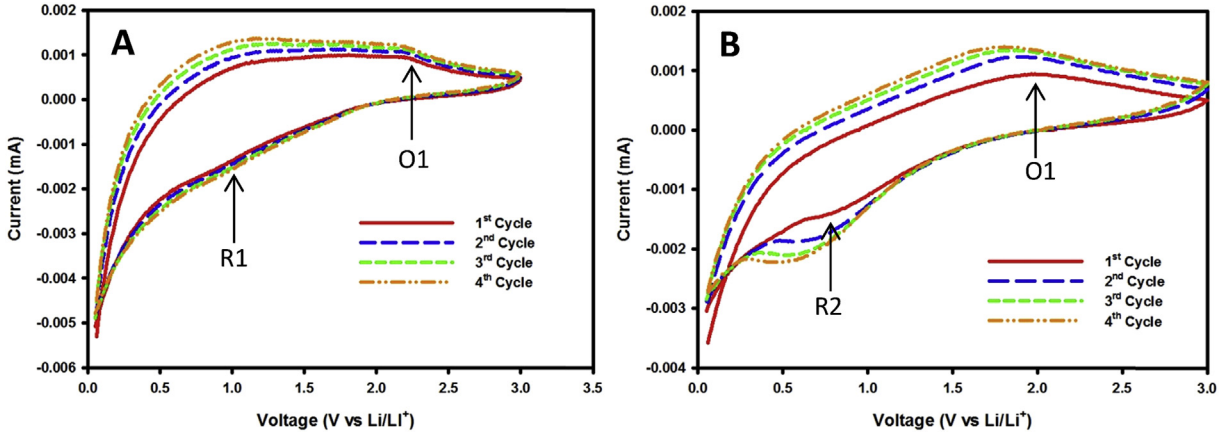

Fig. 10. Cyclic Voltammetry for non-hollow (A) and hollow (B) is was carried out at 0.01 mV/s between 0.05 V and 3 V.

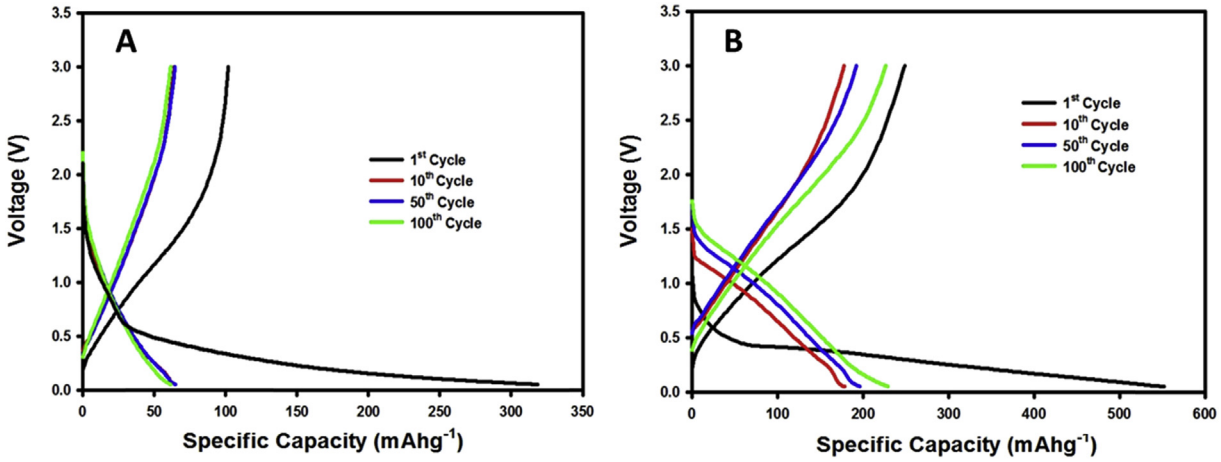

Fig. 11. Charge Discharge profiles for non-hollow (A) and hollow (B) TiO_2/C composite nanofibers carried out at a current density of 100 mAg^{-1}.

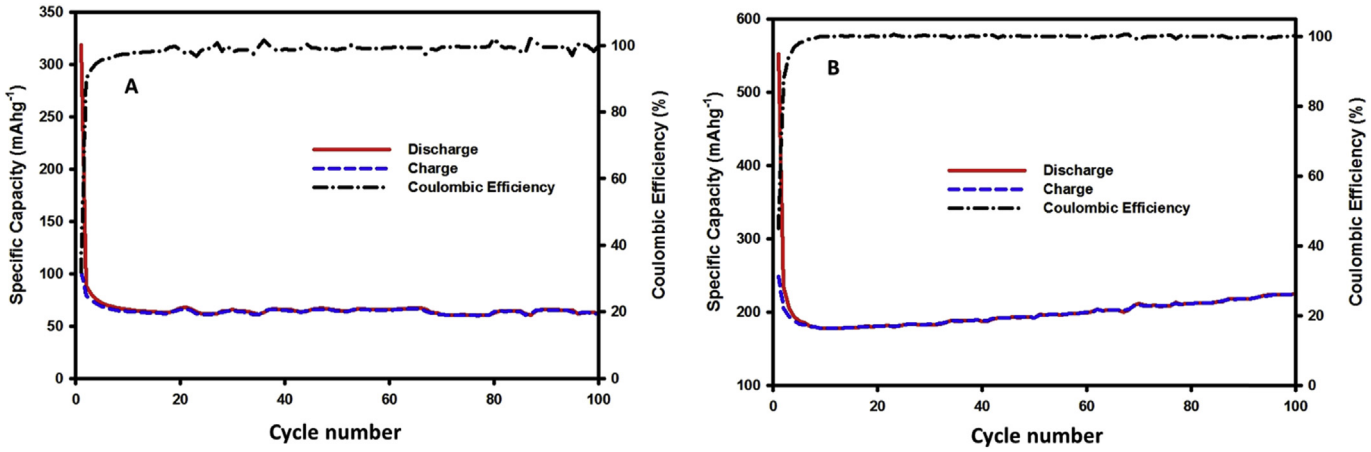

Fig. 12. Cycle performance for 100 cycles at a current density of 100 mAg^{-1} for non-hollow (A) and hollow (B) TiO_2/C nanofibers.

4.3. Cycling performance

The cycling performance was carried out on coin cells for both the non-hollow and hollow fibers, at a current density of 100 mAg^{-1} for 100 cycles as shown in Fig. 12. The electrode from the non-hollow fibers showed an initial specific capacity of 318.3 $mAhg^{-1}$ and a final specific capacity of 61.4 $mAhg^{-1}$ after 100 cycles with an initial coulombic efficiency of 32.03%. Upon cycling, it maintained a coulombic efficiency ~96% over the 100 cycles. On the other hand, the electrode from the hollow fibers showed an improved initial capacity of 552.12 $mAhg^{-1}$ and a final specific capacity of 228.9 $mAhg^{-1}$ after 100 cycles with an initial coulombic efficiency of 45.03%, and then maintaining a coulombic efficiency ~98%. This improvement in electrochemical performance from the multichannel hollow fibers could be attributed to the increase in reactive sites for the Li^+ within the anode. The more stable coulombic efficiency from the hollow fibers also would be due to the hollow structure allowing for safe expansion and contraction of the anode during the alloying/de-alloying and lithium intercalation reactions as shown in Equations (1) and (2). Another feature that was exhibited by the hollow TiO_2/C nanofibers was a recovery of the initially lost capacity compared to the non-hollow fibers whose capacity decreased steadily even after the initial capacity loss.

A comparison of electrochemical performance of TiO_2/C composite electrodes reported in literature is shown on Table 2. This table shows that most results reported prepared by other fiber producing methods show capacities that range from 131 to 680 $mAhg^{-1}$ after cycling. Of the three reports listed that showed higher specific capacity, two were performed at lower current density which results in a higher capacity. The highest performing report which was that of 680 $mAhg^{-1}$ was due to a highly porous microstructure that was achieved by the use of a sacrificial polymer. Some of the reports also use additives such as acetylene black to prepare the composite nanofiber anodes which led to improve the electrical conductivity of the TiO_2-based electrodes [18,20,23,24,34,45].

4.4. Rate performance

The behavior of the electrodes under varying charge density was evaluated by performing a rate capability test (Fig. 13). For this experiment the same coin cell was cycled continuously with varying current density for 10 charge/discharge cycles with a 10 min rest; initially at 50 mAg^{-1} and increased to 100 $mAhg^{-1}$ through to 500 $mAhg^{-1}$. Once the coin cell cycled at a current density of 500 mAg^{-1}, it was then cycled back to the initial current density of 50 mAg^{-1} expecting to exhibit full capacity recovery. The non-hollow TiO_2/C nanofiber anode showed poor rate capacity when cycled at a high current density of 500 mAg^{-1} when compared to the hollow TiO_2/C fiber anode which showed a better

Table 2
Results reported in the literature on the electrochemical performance of bare TiO_2 and TiO_2/C composite nanofiber anodes, for LIBs, prepared by using different methods.

Materials	Method	Performance		Reference
TiO_2/Carbon	Forcespinning®	229 after 100 cycles	At 100 mAg^{-1}	This work
TiO_2/Graphene	Electrospinning	131 after 300 cycles	At 150 mAg^{-1}	[24]
TiO_2/Carbon	Coaxial Electrospinning	680 after 250 cycles	At 100 mAg^{-1}	[34]
TiO_2	Soft-template method	256 after 30 cycles	At 66 mAg^{-1}	[20]
TiO_2	Coaxial Electrospinning/Nitridation	160 after 100 cycles	At 66 mAg^{-1}	[18]
TiO_2	Electrospinning	175 after 50 cycles	At 100 mAg^{-1}	[37]
TiO_2/Carbon	Electrospinning	206 after 100 cycles	At 30 mAg^{-1}	[23]
TiO_2/Carbon	Electrospinning	264 after 100 cycles	At 33 mAg^{-1}	[46]
TiO_2/Graphene	Chemical Synthesis	175 after 100 cycles	at 333 mAg^{-1}	[47]
TiO_2	Electrospinning/Uniaxial pressing	188 after 100 cycles	At 66 mAg^{-1}	[36]
TiO_2/Graphene	Nucleation and growth	153 after 70 cycles	At 150 mAg^{-1}	[45]

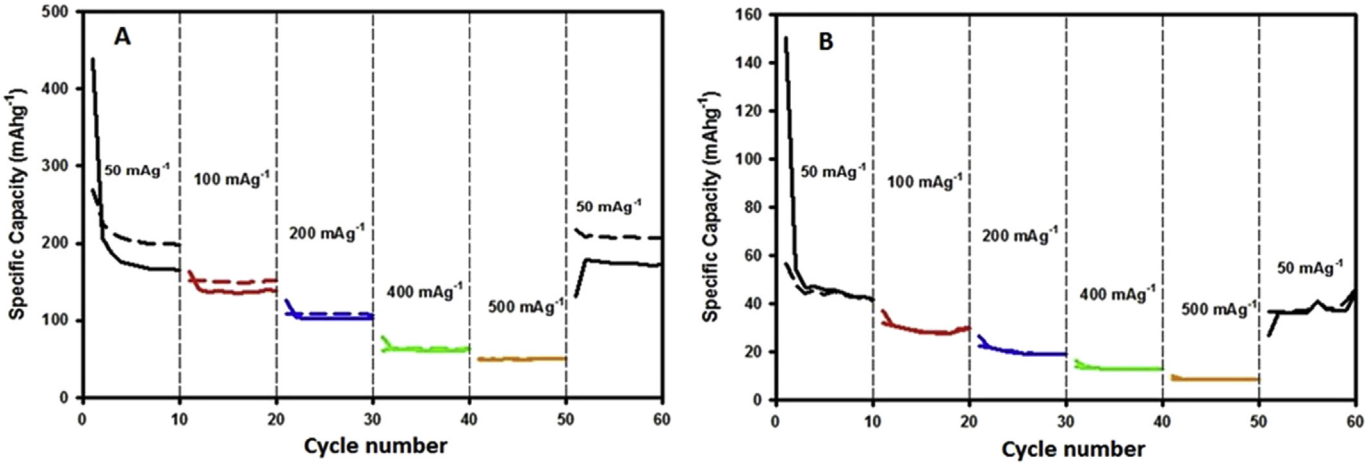

Fig. 13. Rate performance for non-hollow (A) and hollow (B) TiO_2/Carbon nanofibers is shown at current densities of 50, 100, 200, 400 and 500 mAg^{-1}. The solid line represents the discharge capacity (Li insertion) and the dashed line corresponds to the charge capacity (Li de-insertion).

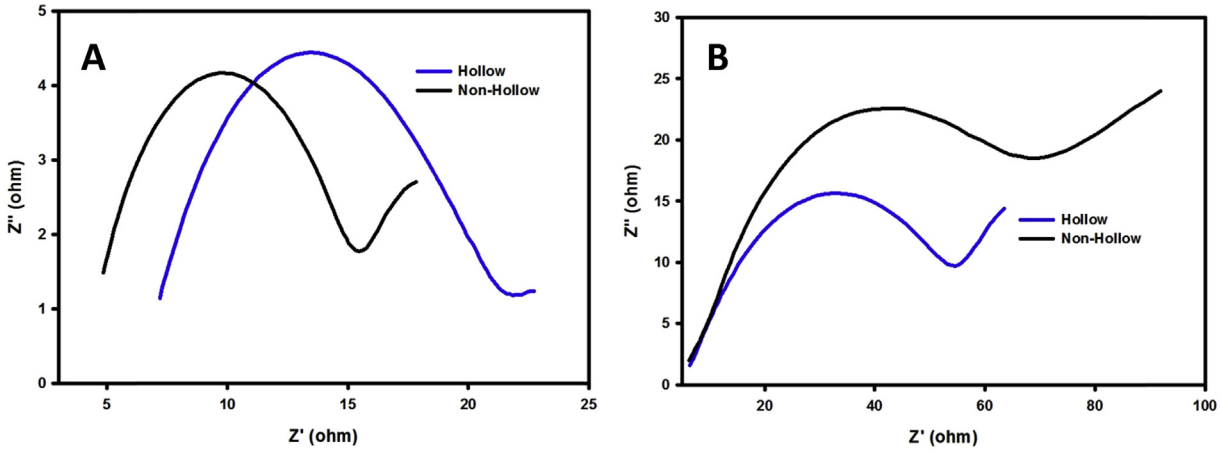

Fig. 14. Nyquist impedance plots for the coin cells containing the hollow and non-hollow TiO_2/C fibers are shown with fresh uncycled cells shown in (A) and aged cells after 100 cycles shown in (B).

specific capacity of 51.2 $mAhg^{-1}$ at 500 mAg^{-1}.

4.5. Impedance

The Nyquist plots for the electrochemical impedance before and after cycling for both the hollow and non-hollow fiber anodes as shown in Fig. 14 were carried out to explain the associated electrochemical performance. The semicircles in the high to mid frequency range represent the initial interfacial resistance and charge-transfer resistance. For the fresh cells which are represented on Fig. 14A, the difference in electrochemical impedance (given by the diameter of the semicircle) was very negligible between the hollow and non-hollow which was only 2.5 Ω. After 100 cycles, there is an increase in the diameter of the semi-circle for both electrodes, with the non-hollow fiber anode having a slightly higher semi-circular diameter meaning higher electrochemical

impedance. The increase in resistance at the electrode/electrolyte interface for the non-hollow fiber anode affected the lithium ion kinetics which is correlated with the steady loss in the cell capacity during the initial cycles and continued to the 100th cycle. On the other hand, the impedance for the hollow TiO_2/C fiber anode increased relative to its corresponding fresh cell impedance, but was lower than its aged counterpart of the non-hollow fiber anode. The improvement in electrochemical performances of the hollow fiber nanofiber anode is attributed to the multichannel hollow microstructure that provided a larger number of active sites for Li^+ storage, and also provided shorter lithium ion transfer distance thus reducing the impedance when cycling.

5. Conclusion

TiO_2/C composite multichannel hollow nanofibers were produced to be used as anodes in LIBs. The nanofibers were prepared by the Forcespinning® of a PVP/Titanium (IV) butoxide/ethanol/acetic acid/mineral oil precursor solution followed heat treatment. This hollow morphology allowed for an improvement in electrochemical performance over non-hollow fibers demonstrating excellent cycling stability, enhanced specific capacity, and excellent capacity retention over 100 cycles. This is the first reported time TiO_2/C nanofibers have been produced via Forcespinning® for the use in LIB's, as well as the first report of using an emulsion solution to manipulate fiber microstructure via Forcespinning®. The use of Forcespinning® shows much promise due to high fiber yield and ease of operation. The enhanced electrochemical performance of the TiO_2/C nanofibers along with the advantages of Forcespinning®, make these nanofibers a very promising candidate for use as next generation anode materials for LIBs.

Acknowledgements

This research is supported by NSF PREM award DMR-1523577: UTRGV-UMN Partnership for Fostering Innovation by Bridging Excellence in Research and Student Success. We would also like to acknowledge Mr.'s Hilario Cortez and Edgar Munoz from the Mechanical Engineering Department at UTRGV for their assistance with the SEM, EDS and XPS analyses. We would also like to thank Mr. Hector De Santiago from the Chemistry Department at UTRGV for the BET surface area and pore size analysis of the composite fibers discussed in this work.

References

[1] J.M. Tarascon, M. Armand, Issues and challenges facing rechargeable lithium batteries, Nature 414 (6861) (2001) 359–367.
[2] V. Agubra, J. Fergus, Lithium ion battery anode aging mechanisms, Materials 6 (4) (2013) 1310.
[3] J. Xu, et al., Cathode materials for next generation lithium ion batteries, Nano Energy 2 (4) (2013) 439–442.
[4] J. Chen, et al., Sn-contained N-rich carbon nanowires for high-capacity and long-life lithium storage, Electrochim. Acta 127 (0) (2014) 390–396.
[5] H. Park, et al., Electrospun Li4Ti5O12 nanofibers sheathed with conductive TiN/TiOxNy layer as an anode material for high power Li-ion batteries, J. Power Sources 244 (0) (2013) 726–730.
[6] G. Zhang, et al., Tin quantum dots embedded in nitrogen-doped carbon nanofibers as excellent anode for lithium-ion batteries, Nano Energy 9 (2014) 61–70.
[7] M. Alcoutlabi, L. Banda, G.B. McKenna, A comparison of concentration-glasses and temperature-hyperquenched glasses: CO2-formed glass versus temperature-formed glass, Polymer 45 (16) (2004) 5629–5634.
[8] M. Alcoutlabi, et al., Electrospun nanofibers for energy storage, Aatcc Rev. 11 (6) (2011) 45–51.
[9] V.A. Agubra, L. Zuniga, D. De la Garza, L. Gallegos, M. Pokhrel, M. Alcoutlabi, Forcespinning: a new method for the mass production of Sn/C composite nanofiber anodes for lithium ion batteries, Solid State Ionics 286 (2016) 73–82.
[10] L.W. Ji, et al., Recent developments in nanostructured anode materials for rechargeable lithium-ion batteries, Energy & Environ. Sci. 4 (8) (2011) 2682–2699.
[11] V.A. Agubra, et al., Composite nanofibers as advanced materials for Li-ion, Li-O-2 and Li-S batteries, Electrochim. Acta 192 (2016) 529–550.
[12] Y. Domi, et al., In situ AFM study of surface film formation on the edge plane of HOPG for lithium-ion batteries, J. Phys. Chem. C 115 (51) (2011) 25484–25489.
[13] J.S. Gnanaraj, et al., Formation and growth of surface films on graphitic anode materials for Li-Ion batteries, Electrochem. Solid-State Lett. 8 (2) (2005) A128–A132.
[14] L. Hardwick, An Investigation of the Effect of Graphite Degradation on the Irreversible Capacity in Lithium-ion Cells, 2008.
[15] W. Xia, et al., Facile approach to synthesize SnO2 nanoparticles@carbon nanofibers as anode materials for lithium-ion battery, J. Power Sources 217 (0) (2012) 351–357.
[16] Q. Yang, et al., Enhanced performance of SnO2–C composite fibers containing NiO as lithium-ion battery anodes, Ceram. Int. 41 (9, Part A) (2015) 11213–11220.
[17] J. Zhu, et al., SnO2 nanorods on ZnO nanofibers: a new class of hierarchical nanostructures enabled by electrospinning as anode material for high-performance lithium-ion batteries, Electrochim. Acta 150 (0) (2014) 308–313.
[18] C.A. Bonino, et al., Electrospun carbon-tin oxide composite nanofibers for use as lithium ion battery anodes, Acs Appl. Mater. Interfaces 3 (7) (2011) 2534–2542.
[19] W. Luo, et al., Surface modification of electrospun TiO2 nanofibers via layer-by-layer self-assembly for high-performance lithium-ion batteries, J. Mater. Chem. 22 (11) (2012) 4910–4915.
[20] K. Saravanan, K. Ananthanarayanan, P. Balaya, Mesoporous TiO2 with high packing density for superior lithium storage, Energy & Environ. Sci. 3 (7) (2010) 939–948.
[21] L. Li, J.B. Zhang, Q.S. Zhu, A novel fractional crystallization route to porous TiO2-Fe2O3 composites: large scale preparation and high performances as a photocatalyst and Li-ion battery anode, Dalton Trans. 45 (7) (2016) 2888–2896.
[22] J. Liang, et al., A graphene–SnO2–TiO2 ternary nanocomposite electrode as a high stability lithium-ion anode material, J. Alloys Compd. 673 (2016) 144–148.
[23] Z.X. Yang, et al., Synthesis of uniform TiO2@carbon composite nanofibers as anode for lithium ion batteries with enhanced electrochemical performance, J. Mater. Chem. 22 (12) (2012) 5848–5854.
[24] X. Zhang, et al., Electrospun TiO2-graphene composite nanofibers as a highly durable insertion anode for lithium ion batteries, J. Phys. Chem. C 116 (28) (2012) 14780–14788.
[25] Y. Li, et al., Fabrication of TiO2 hollow nanostructures and their application in Lithium ion batteries, J. Alloys Compd. 651 (2015) 685–689.
[26] Z.H. Chen, et al., Titanium-based anode materials for safe lithium-ion batteries, Adv. Funct. Mater. 23 (8) (2013) 959–969.
[27] J. Liang, et al., Fabrication of TiO2 hollow nanocrystals through the nanoscale Kirkendall effect for lithium-ion batteries and photocatalysis, New J. Chem. 39 (4) (2015) 3145–3149.
[28] S. Li, et al., Anchoring ultra-fine TiO2-SnO2 solid solution particles onto graphene by one-pot ball-milling for long-life lithium-ion batteries, J. Mater. Chem. A 3 (18) (2015) 9700–9706.
[29] H.T. Fang, et al., Comparison of the rate capability of nanostructured amorphous and anatase TiO2 for lithium insertion using anodic TiO2 nanotube arrays, Nanotechnology 20 (22) (2009) 0957–4484.
[30] P. Zhu, et al., Long term cycling studies of electrospun TiO2 nanostructures and their composites with MWCNTs for rechargeable Li-ion batteries, RSC Adv. 2 (2) (2012) 531–537.
[31] M.C. Yang, et al., TiO2 flakes as anode materials for Li-ion-batteries, J. Power Sources 207 (2012) 166–172.
[32] C. Lai, et al., Mesoporous polyaniline/TiO2 microspheres with core–shell structure as anode materials for lithium ion battery, J. Power Sources 196 (10) (2011) 4735–4740.
[33] Z. Guo, et al., A core-shell-structured TiO2(B) nanofiber@porous RuO2 composite as a carbon-free catalytic cathode for Li-O2 batteries, J. Mater. Chem. A 3 (42) (2015) 21123–21132.
[34] F. Wang, et al., Porous tin film synthesized by electrodeposition and the electrochemical performance for lithium-ion batteries, Electrochim. Acta 149 (0) (2014) 330–336.
[35] K. Tang, et al., Multichannel hollow TiO2 nanofibers fabricated by single-nozzle electrospinning and their application for fast lithium storage, Electrochem. Commun. 28 (2013) 54–57.
[36] S. Lee, et al., 3D cross-linked nanoweb architecture of binder-free TiO2 electrodes for lithium ion batteries, Acs Appl. Mater. Interfaces 5 (22) (2013) 11525–11529.
[37] P. Tammawat, N. Meethong, Synthesis and characterization of stable and binder-free electrodes of TiO2 nanofibers for Li-Ion batteries, J. Nanomater. 2013 (2013) 8, http://dx.doi.org/10.1155/2013/413692. Article ID 413692.
[38] K. Sarkar, et al., Electrospinning to Forcespinning™, Mater. Today 13 (11) (2010) 12–14.
[39] V.A. Agubra, et al., ForceSpinning of polyacrylonitrile for mass production of lithium-ion battery separators, J. Appl. Polym. Sci. (1) (2016) 133.
[40] B.C. Weng, et al., Fibrous cellulose membrane mass produced via force-spinning(A (R)) for lithium-ion battery separators, Cellulose 22 (2) (2015)

1311–1320.
[41] B.C. Weng, et al., The production of carbon nanotube reinforced poly(vinyl) butyral nanofibers by the forcespinning (R) method, Polym. Eng. Sci. 55 (1) (2015) 81–87.
[42] X. Wang, et al., Facile scalable synthesis of TiO2/carbon nanohybrids with ultrasmall TiO2 nanoparticles homogeneously embedded in carbon matrix, Acs Appl. Mater. Interfaces 7 (43) (2015) 24247–24255.
[43] K.H. Seng, et al., Catalytic role of Ge in highly reversible GeO2/Ge/C nano-composite anode material for lithium batteries, Nano Lett. 13 (3) (2013) 1230–1236.
[44] X.J. Bai, et al., Preparation and electrochemical properties of profiled carbon fiber-supported Sn anodes for lithium-ion batteries, J. Alloys Compd. 628 (2015) 407–412.
[45] J.W. Wang, et al., Two-phase electrochemical lithiation in amorphous silicon, Nano Lett. 13 (2) (2013) 709–715.
[46] M.H. Ryu, et al., High performance N-Doped mesoporous carbon decorated TiO2 nanofibers as anode materials for lithium-ion batteries, J. Phys. Chem. C 117 (16) (2013) 8092–8098.
[47] X. Xin, et al., Scalable synthesis of TiO2/graphene nanostructured composite with high-rate performance for lithium ion batteries, Acs Nano 6 (12) (2012) 11035–11043.